EB2020-STP-002

Design, Set-up and Validation of an Aerodynamic Bench for Wheel Corner Flow Investigation in Vented Brake Discs Testing

Samaneh Rouina [1*], Giovanna Barigozzi [1], Paolo Iavarone [2], Andrea Milesi [2], Fabrizio Venanzoni [3], Gabriele Riva [3]

[1] *Univeristà degli studi di Bergamo, Italy*
[2] *BSCCB, Italy*
[3] *Brembo S.p.A, Italy*

https://doi.org/10.46720/EB2020-STP-002

ABSTRACT: Brake disc cooling is strongly affected by the aerodynamic condition surrounding the system and especially by the flow at the ventilation channels inlet. Aero-thermal performance of brake discs are usually tested using a dyno bench in which the aerodynamic field is not representative of the one in the wheel corner of car vehicles. The purpose of this study is to design a dyno bench configuration, called aero-dynamic bench, whose airflow replicates the cooling distribution seen in a vehicle wheel corner. A carbon-ceramic brake disc (CCM) and an aluminum caliper of a sports car are considered for the design. The work can be summarized into three steps. The first step consists of a computational fluid dynamic (CFD) analysis of the dyno bench. The second step involves the realization of the new dyno bench facility starting from the standard one and calibrating the air supply systems. Third, the flow field at the outlet of the ventilation channels is measured by means of Laser Doppler Anemometry (LDA) as well as hot-wire anemometry (HWA). Experimental results are qualitatively in line with CFD analysis and reveal that installing the brake disc in the wheel corner results in a vented air mass flowrate reduction. Moreover, the presence of forced convection, compared with the disc auto-ventilation condition, makes the flow exiting the disc channels more uniform as well as with a reduced turbulence intensity level.

KEY WORDS: brake disc, brake cooling, LDA, HWA, CFD.

1. Introduction

Nowadays, vented brake discs are widely used in automotive industry due to their better heat transfer performance with respect to the solid ones. There has always been much effort to improve heat dissipation rate of these rotors which leads to a smaller and lighter design. One determining aspect in a rotor heat dissipation is airflow exiting the rotor itself. Many studies have been conducted to measure the airflow in the laboratories using different measurement techniques [1-5]. Barigozzi et al. [1,2] have investigated aerothermal behaviour of the airflow at the exit of vented brake discs using hot-wire anemometry (HWA) and cold wire (CWT) techniques. They revealed that nor the flow regime neither the disc surface temperature variation alter the airflow structure at the channel exits, which is usually characterized by a classical jet and wake flow pattern. Their studies also pointed out to the fact that the higher the disc surface temperature is the less the vented mass flow rate, due to the higher exiting air density ratio. Furthermore, the air temperature distribution supports the flow field measurements at the channel exit. In another study [3], CCM vented brake discs with cross-drilled holes have been investigated. This study confirmed [1,2] and have also shown that the holes on the disc have contributed to the 22% of the overall vented air. Johnson et al. [4] examined the flow field at the inlet and exit of the brake disc, as well as inside the cooling passages using a two-component PIV system. They captured the presence of large separation areas in the air passages which cause poor cooling performance of the rotor. Furthermore, Parish et al. [5] investigated the unsteady flow field of a variety of vented brake discs making use of the HWA technique. They found that the rotor mass flow rate varies linearly with the rotational speed, and confirmed the passage-to-passage jet-wake region in the exit flow field with a high level of unsteadiness in the wake region. In addition to experimental studies, many computational studies have been investigated the cooling performance of brake discs [6-9]. Voller et al. [8], and Barigozzi et al. [9] performed combined experimental and numerical investigations of brake disc cooling characteristics, and they showed that CFD predictions in terms of heat transfer coefficient were consistent with experimental data. Most of the previous works concerning the brake discs in the open literature, either experimental or numerical investigations, have been conducted without considering any obstruction at the inlet or outlet of the disc brakes in still air. Instead, in a real situation, the rotor inlet could be blocked by other car components such as wheel hub, and the heat dissipation of the rotor could be affected by the air around it due to the car forward movement. For example, Watkins et al. [10] investigated airflow through vented brake disc either in still air or moving air using a high frequency cobra probe, and showed an airflow reduction in the latter case.

The focus of this study is to take advantage of a combined numerical and experimental approach to desing and realize a dyno bench which simulates as close as possible the wheel corner flow

in a moving vehicle car. Then, advanced and precise measurement techniques such as LDA and HWA have been used to investigate the influence of forced convection on the flow field at the ventilation channels outlet, and finally validate the numerical models against experinmental data.

2. Experimental Details

The experimental set-up that has been used in this study is an aerodynamic bench that has been realized from an available test bench at the Energy Systems and Turbomachinery Laboratory of the University of Bergamo. For more details regarding the existing test bench, please refer to [1], and the details of new experimental set-up will be presented in section 4.2. The tested disc was the Standard CCM disc with X-drilling which is characterized by a periodical internal structure made up of three radial channels as shown in Figure 1. This periodic sector extends over 36° in the circumferential direction. The first and the third channel have the same circumferential extension whereas the middle one has a smaller outlet area. Concerning the experimental measurements, a 2 component Laser Doppler Anemometer (LDA) has been used to obtain the mean and turbulent flow field distribution over a measurement plane located at a radial distance of 4 mm from the disc outlet border at a fixed rotational speed of 1000 rpm. In particular, radial and tangential velocity components have been measured, which leads to the calculation of turbulence intensity level:

$$Tu = 100.\frac{\sqrt{0.5\,(U'^2_{rad}+U'^2_{tan})}}{U_p} \quad (1)$$

where U_p is the disc peripheral speed computed at the disc external radius R_2, U'_{rad} and U'_{tan} are the root mean square of radial and tangential fluctuating velocity components, respectively. The measurement grid covers most of the disc thickness; it includes 17 measuring points along the disc thickness while interval between points decreases approaching the channel boundaries. A magnetic pick-up provided a once per revolution trigger signal, allowing the phase locked acquisition of LDA samples. Table 1 summarizes the measurement uncertainty.

Table 1 – Measurement uncertainties.

δU LDA	± 2 %
Flow angle	± 1°
Probe position	± 0.1 mm
δU HW	± 3 %

The obtained results have been used to calculate the vented air mass flow rate at channel exit, using equation 2.

$$\dot{m} = \int_A \rho U_{rad} dA = \int_{Y_{min}}^{Y_{max}} \int_{\theta_1}^{\theta_2} \rho U_{rad} dY R d\theta \quad (2)$$

where Y_{min} and Y_{max} and θ_1 and θ_2 identify the channel axial limits and circumferential extension, respectively. A constant air pressure of 1.01325 bar was used while air temperature was changed according with the specific test condition.

For validation purposes, some tests were also repeated using a single wire Hot Wire Anemometer (DANTEC 55P11 probe) and the multi-rotation technique. Hot Wire anemometry (HWA) directly measures the air flow velocity. The only drawback is its sensitivity to temperature variation and the fact that it measures all the flow, i.e. the flow exiting the channels and those entrained by the disc rotation. For more details on measurement techniques and their uncertainity, please refer to [3].

Figure 1 The standard CCM brake disc.

3. Numerical Details

In this section, the description of the numerical approach used to assess the experimental tests is presented in details. The numerical activity consists of steady CFD simulations by using Siemens STAR CCM+ software [11]. The aim of the numerical simulations is to obtain the aerodynamic field in terms of pressure and velocity around the braking system, by giving as input the real boundary conditions of the domain at inlets, outlets and walls. A CAD model of the experimental set-up has been used to perfectly reproduce the geometry of the aerodynamic domain, including the whole braking system and the wheel. The geometrical domain is discretized into polyhedral mesh cells and the software solves the Navier Stokes Equations in the volume mesh by using the Finite Volume Method [12]. The number of volume cells for this model is 7,562,000. The chosen solver is of the RANS type. The Reynolds-averaged Navier Stokes equations (or RANS equations) [13] are time-averaged equations of motion for turbulent fluid flows. These equations are based on Reynolds decomposition, which decomposes an instantaneous quantity into its time averaged and fluctuating quantities. For a stationary, incompressible Newtonian fluid, these equations can be written in Einstein notation in Cartesian coordinate as:

$$\rho\overline{u_j}\frac{\partial\overline{u_i}}{\partial x_j} = \rho\overline{f_i} + \frac{\partial}{\partial x_j}\left[-\bar{p}\delta_{ij} + \mu\left(\frac{\partial\overline{u_i}}{\partial x_j}+\frac{\partial\overline{u_j}}{\partial x_i}\right) - \rho\overline{u_i'u_j'}\right] \quad (3)$$

The non linearity of the fluctuating component (i.e. the tensor of Reynolds stresses) requires a model to close the equations. In this simulation the k-ε turbulence closure model has been used. The k-ε model provides a description of turbulence by using two partial differential transport equations. The first variable transported is k, i.e. the turbulent kinetic energy, and the second is ε, the turbulent energy dissipation rate. The simulation is stationary, three-dimensional, and the air is treated as an ideal gas, with a segregated flow model. The viscosity of the fluid is a function of temperature, and in the case of air, the relationship is determined by the Sutherland's law:

$$\frac{\mu}{\mu_0} = \frac{T}{T_0}^{1.5}\frac{T_0+110}{T+110} \quad (4)$$

where:

T_0 = 288 K, and μ_0 = 1.79e $^{-5}$ Kg/ms.

The wall flow treatment is based on the use of wall functions with an all-y+ approach. In this treatment, a separate expression is used for the buffer layer that blends smoothly with the viscous and inertial layer expressions. When the cell centroid falls within the buffer layer, this modeling approach will produce more accurate results relative to the high Re approach. There are no grid size obligations with this wall treatment. A rotating local reference system has been created which is integral with the braking disc, to simulate rotation. The center of the reference system coincides with the center of the disc and lies in the middle plane of the thickness of the ventilation. An angular velocity has been assigned to this rotating region equal to 1000 rpm.

The case study is the operating condition of forced convection with all the lines on, which is the most similar to the real vehicle condition. Inlet temperature sets equal to 25 °C, ambient pressure is 1.01325 bar. Mass flow boundary conditions for each air line for the simulation were applied as measured by LDA technique during experiments.

4. Design, Set-up and Validation of the Aerodynamic Bench

In this section, the numerical analysis that has been done to realize the aero-dynamic bench is presented. Also, the results of the measurement campaign that has been carried out to validate its cooling system mass flowrate are discussed in details. The authors decided to present these kind of results in the methodology section because they have been used to develop the aero-dynamic bench configuration. Results obtained for the final configuration will be presented in the results section.

4.1. Numerical Studies

The first target of the numerical analysis has been the definition of an aerodynamic set-up able to describe the convective cooling of a braking system in terms of Heat Transfer Coefficients (HTC). This set-up has to be able to replicate the distribution of HTCs on the caliper and the disc of a real moving vehicle. The software calculates the Navier-Stokes equations at each iteration and uses the thermal power exchanged as input to obtain the values of HTC based on the temperature boundary conditions, thus resulting:

$$HTC = \frac{\dot{q}}{T_{wall} - T_{fluid}} = h(x, y, z, v) \qquad \left[\frac{W}{m^2 K}\right] \qquad (5)$$

where $\dot{q}$ is the thermal power exchanged per unit of area, T_{wall} is the body wall temperature, and T_{fluid} is the temperature of the fluid in contact with the wall.

The starting point of the activity has been a CFD analysis of a vehicle submodel, limited to the front wheel compartment, performed directly by a car maker company (Fig. 2a). This model, previously correlated with the CFD analysis of the whole vehicle, has been used to extract values of temperature, velocity and pressure on the walls of the wheel compartement. This has been done for two different values of car speed. These parameters have been used as boundary conditions for a set of steady CFD simulations aimed at defining the correct set-up needed to obtain a HTC distribution as close as possible to the real one. The physical model used in these simulations is the one described in section 3. The first configuration included only the rotating components, then an injection pipe has been introduced to simulate forced convection on the disc (Fig. 2b). These simulations have been used to decide how to simulate the rotation of the disc. The choice fell on the use of a rotating air domain surrounding the disc and the wheel, because of the more accurate results in terms of heat transfer on the braking surfaces coupled with an acceptable computational cost. Still being far from a realistic correlation, a new configuration has been developped in the model, consisting of three air blowing lines and a suction hood (Figure 2c).

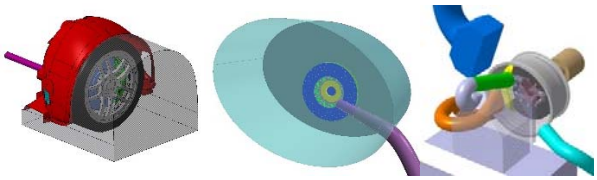

(a) (b) (c)

Figure 2 (a) CAD Design of the vehicle submodel, (b) single pipe configuration, (c) final layout.

Several simulations have been performed by varying the position of the pipes, until the final layout has been accepted for the model assessment. Figure 3 shows the comparison between HTC distributions in the newly designed dyno bench model and in the vehicle submodel. This final layout has been the basis for the experimental activity, as well as for the numerical CFD steady simulations performed to be compared with the experimental results as presented in Section 5.

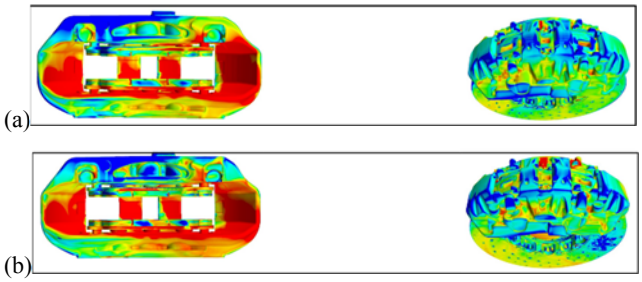

(a)

(b)

Figure 3 (a) HTC distribution in vehicle submodel, (b) HTC distribution in the aerodynamic bench.

4.2. Aero-dynamic bench Set-up

After thorough numerical analysis, the realization of the aero-dynamic bench has been done starting from the existing one, in order to obtain a test facility that replicates as much as possible the geometrical and flow conditions of a moving vehicle. For this purpose, the rim, the wheel bearing, the wheel hub, and vehicle suspension have been incorporated into the disc brake and the brake and pad system along with a solid block that represents the car body in a real situation (See Figure 4).

Furthermore, the three blowing air lines of the simulated dyno bench have been added to the test bench to simulate the airflow around the brakes in a moving vehicle as shown in Figure 5 (a). In particular, Line#1 drives air to the caliper, Line#2 to the disc inlet

and Line#3 to the friction surface. In addition, one lateral suction hood has been added to the whole system to discharge the air outside (See Figure 5(b)). Figure 6 shows the existing test bench and the new one with all applied modifications. For mass flow rate verification, LDA technique has been used to measure the axial velocity component (U_{ax}) of the airflow exiting from each line.

Figure 7 shows the measured axial velocity profiles along the pipe diameter of the three lines. Table 2 summarizes the differences between measured and desired mass flowrate for all three lines. These values show that a good match has been obtained concerning both Line#1 and #2 while a too large mass flow is provided during measurements through Line#3.

(a) (b) (c)

Figure 4 The disc and pad system with the car components; (a) CAD Design, (b) the Test Bench.

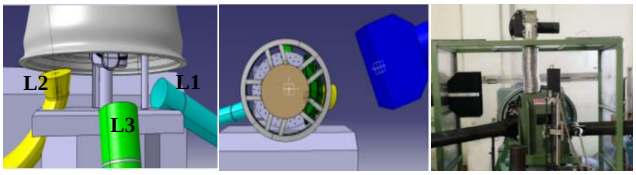

(a) (b) (c)

Figure 5 (a) CAD Design for three blowing air lines, (b) the lateral hood CAD Design, (c) final layout.

(a)

(b)

Figure 6 (a) the existing test bench, (b) the developed test bench.

Table 2 Comparison of measured mass flowrate with requested data.

	$\Delta\dot{m}/\dot{m}$ %
Line#1	-17.4
Line#2	1.2
Line#3	45.5

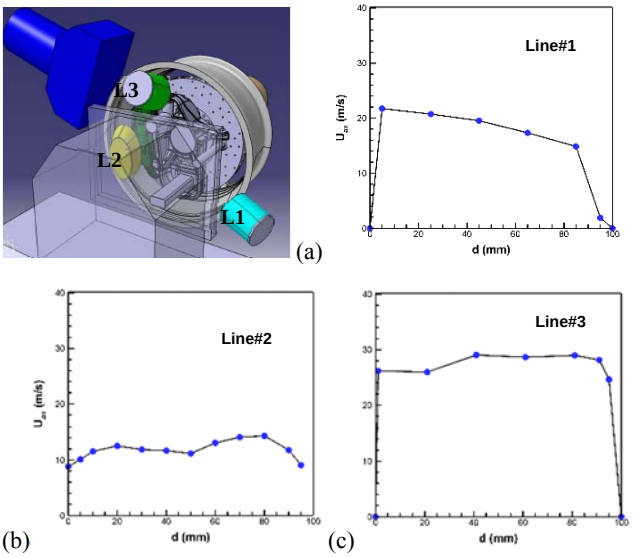

(a) (b) (c)

Figure 7 Axial velocity profiles measurement for: a) Line#1, b) Line#2 and c) Line#3.

5. Results and Discussion

5.1. Air line sensitivity analysis

The test bench has been verified, evaluating the influence of each air line flow on the disc vented air. This has been done to ensure the correct position and blowing direction of each air line. In order to do this, LDA measurements have been performed at a distance of 4 mm from channel outlet with one fan in operation at a time, and with the disc roating at a fixed rotational speed of 1000 rpm. Distribution of normalized radial velocity and its corresponding turbulence intensity level for all cases are presented in Figure 8 and 9, respectively. Each contour plot shows the phase averaged distribution of radial velocity component (U_{rad}) and turbulence intensity level (Tu%) at the exit of the three venting channels that constitute a disc periodic sector. The radial velocity has been normalized using the disc peripheral speed U_p while turbulence intensity level has been normalized using its mean value with all fans off.

The measured flow structure is consistent with the disc periodic structure made of three channels. It has to be reminded that the first and the third channel have the same circumferential extension whereas the middle one has a smaller outlet area. First considering the no blowing case of Fig. 8 (a) & 9 (a), the typical “jet & wake” behavior characterizes all three channels: starting from the left end side, the low velocity region around θ=0° indicates the presence of the first blade. The first channel flow field has two peaks: the first one, of reduced intensity, is located close to the blade suction side while the second one is located on the channel pressure side, close to the next blade wake around θ=12°-14°. A similar two-peak structure also characterizes the two following channels, even if the third one shows reduced velocity values, due to the worst inlet condition for this channel. The turbulence intensity contour plots of Fig. 9 (a) show high Tu values in the wake regions behind the blades and at the channels boundaries. Low Tu values are instead

detected in the central portion of all channels. The middle channel shows the lowest values, testifying a more organized flow structure.

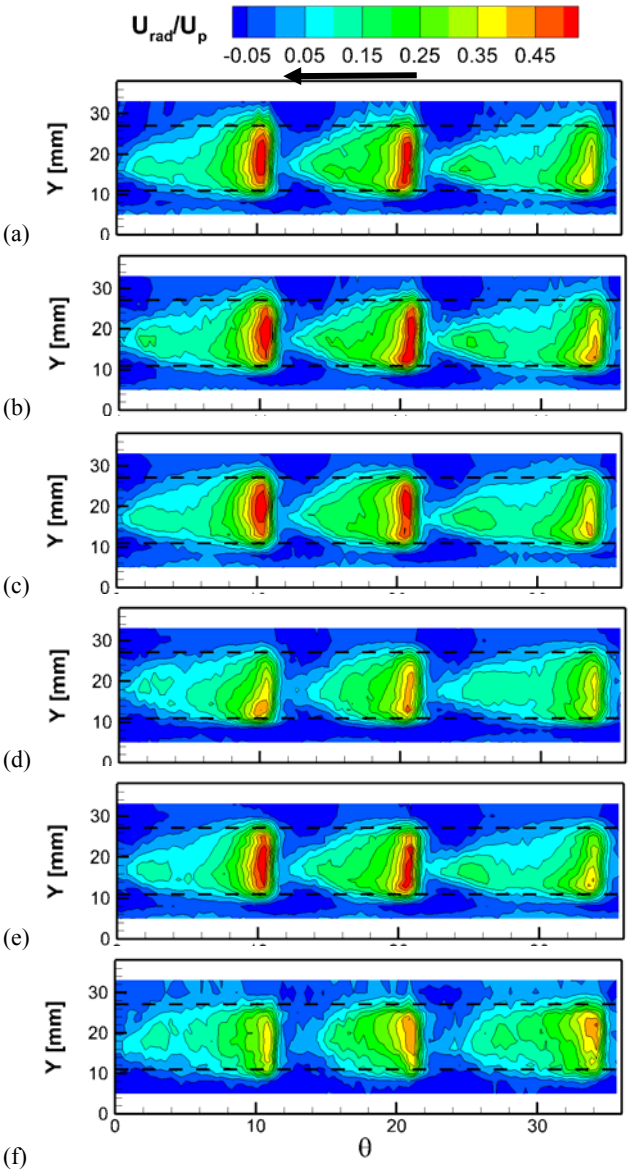

Figure 8 Radial velocity distributions at 1000 rpm, a) all off, b) Line#1 on, c) Line#2 on, c) Line#3 on, d) hood on and e) all on.

Now comparing the different operating conditions reported in Fig. 8 & 9, only minor differences are detected: a general slight decrease both in the radial velocity and turbulence intensity level is observed when the fans are put in operation, whatever the fan blowing, even if the general flow structure remains unchanged. Line#3 (Fig. 8 (c) & 9 (c)) leaves the largest impact on the radial velocity and turbulence intensity distributions: both show reduced values. This is due to the fact that Line#3 flow impinges on the disc friction surface, interacting with X-drilling. On the other hand, Line#1 (Fig. 8 (b) & 9 (b)), Line#2 (Fig. 8 (c) & 9(c)) and the suction Hood (Fig. 8 (e) & 9 (e)) all independently create the same flow structure. Finally, when all fans are blowing (Fig. 8 (f) & 9 (f)), the flow pattern is similar to those of Fan#3 alone, but with slightly increased levels, testifying the relevance of this fan in the definition of the disc blowing behavior. Of course, this is also due to the quite large massflow rate characterizing Line#3.

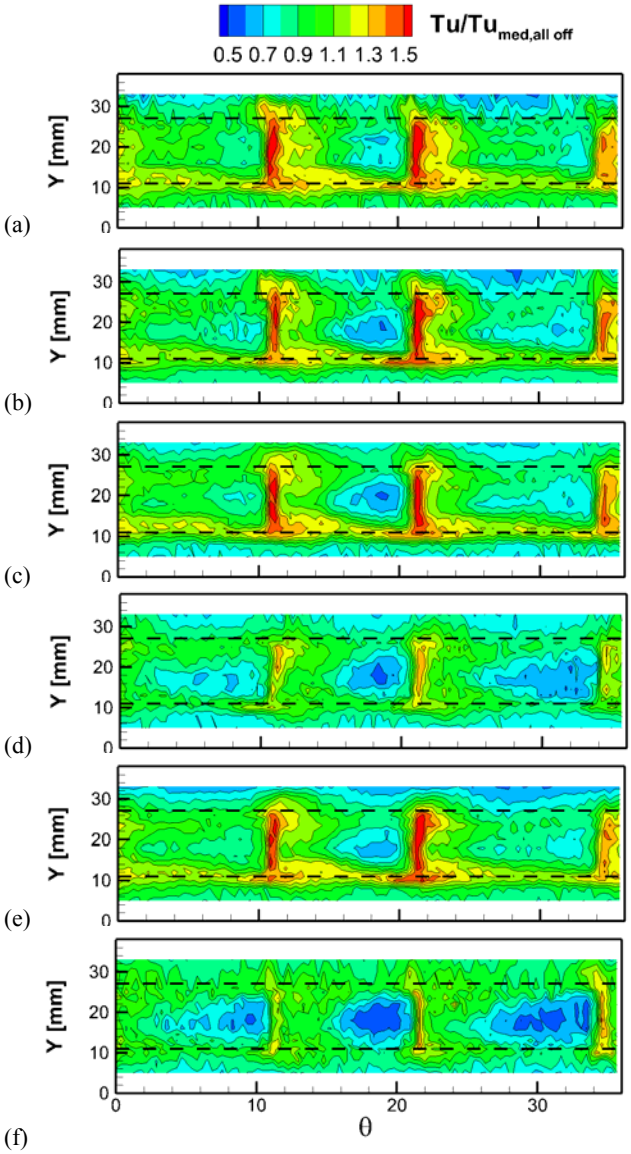

Figure 9 Turbulence Intensity distributions at 1000 rpm, a) all off, b) Line#1 on, c) Line#2 on, d) Line#3 on, e) hood on and f) all on.

By integrating the local radial velocity distributions over the disc exit section, the vented mass flow rate for each case has been computed. Results reported in Table 3 are referred to the case with all Lines off. These results confirm that Line#3, due to its position and large mass flow, has a profound impact on the vented air mass flow rate, therefore its position and blowing direction were carefully checked before running any futher test. In particular, its position was slightly changed in all the following tests, in order to minimize its impact on the vented air mass flow.

5.2. LDA versus HWA cross validation

The cooling lines assessed by means of the LDA technique, vented air flow field investigations have been repeated in the presence of

forced convection at the fixed rotational speed of 1000 rpm using both LDA and HWA techniques for cross validation. In fact, due to the multiple airflow sources, a certain dependency on seeding generation was observed when operating with all fans blowing. The obtained results are presented in terms of normalized radial velocity and turbulence intensity in Figure 10 and 11. Worth to mention the fact that HWA technique directly measures the air velocity, while LDA technique measures the seeding velocity. A further difference is that HWA also feels the entrained air, while LDA only measures particles travelling across the channels. Nevertheless, both give almost the same flow structure at channel exit in terms of radial velocity distribution. The main difference relays in the lower turbulence levels measured by the HWA. The higher turbulence intensity levels measured by LDA could be due to seed generation and distribution at the disc inlet, which might have lead to some perturbation of the exiting airflow.

Table 3 Vented air flow rates (periodic sector).

Forced Convection	$\Delta\dot{m}/\dot{m}$ %
Line#1	0.44
Line#2	-0.73
Line#3	-17.8
Hood	-0.2
All	-8.8

Now comparing Fig. 10 and 11 to Fig. 8 (f) & 9 (f), the new positioning of Fan#3 allowed for slightly larger radial velocity values and a more uniform velocity distribution at channel outlet, compared to the still air case (Fig. 8 (a) & 9 (a)).

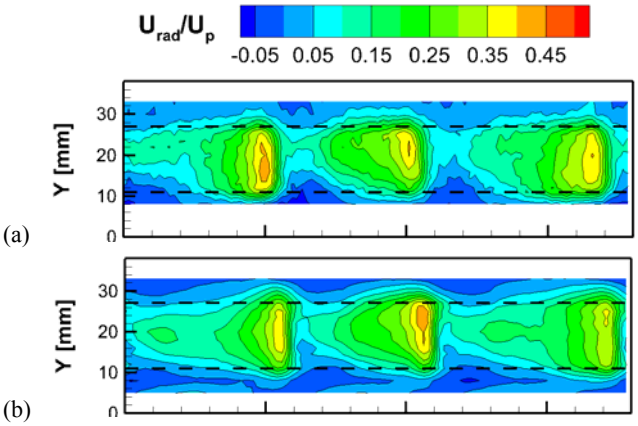

Figure 10 Radial velocity distributions at 1000 rpm with forced convection: a) LDA and b) HWA.

Figure 12 finally reports the normalized radial velocity component and turbulence intensity distribution obtained through the HWA technique testing the disc without forced convection. In particular, Tu contour plot confirms the decrease in turbulence intensity levels with forced convection already evidenced by the LDA technique.

For all cases, local radial velocity component distributions were used to compute the vented mass flow rate through the periodic sector using equation (2) as given in Table 4. Here all values are referred to the one measured with LDA without forced convection. A general agreement between the two approaches can be observed even on the integral values, with a 2.1% difference in the vented mass flow rate with all the fans off. This value is consistent with measurement uncertainty. One could conclude that adding forced convection to the system reduces the air mass flowrate exiting the ventilation channels of about 3.5% with the present setup.

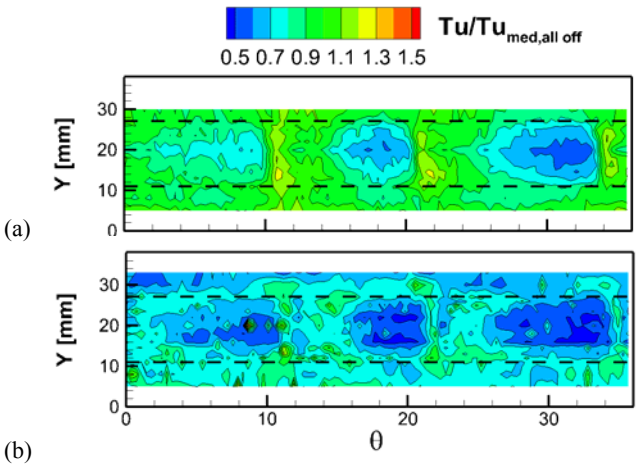

Figure 11 Turbulence intensity distributions at 1000 rpm with forced convection: a) LDA and b) HWA.

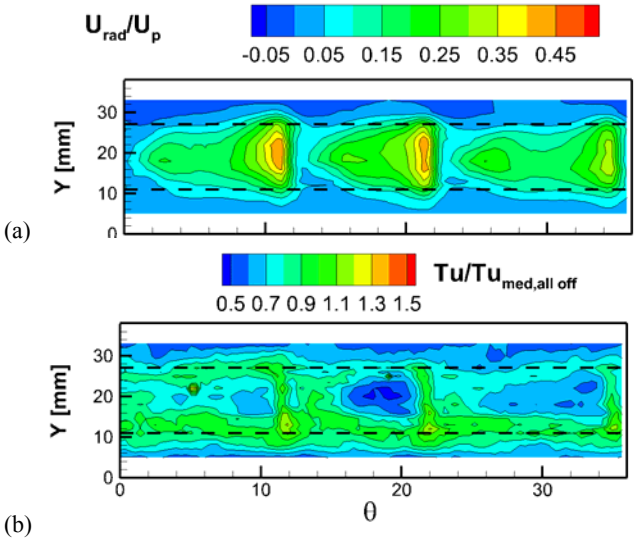

Figure 12 (a) Radial velocity and (b) Turbulence intensity distribution w/o forced convection from HWA.

Table 4 Vented air flow rates (periodic sector).

Forced Convection	$\Delta\dot{m}/\dot{m}$ %	Technique
Yes	-3.5	LDA
No	-2.1	HWA
Yes	-5.1	HWA

Finally, Figure 13 reports the normalized radial velocity and turbulence intensity distributions measured on the same disc but in the original test rig, i.e. with just the disc and the caliper.

Comparing these results with those reported in Fig. 8 (a) & 9 (a) (and also in Fig. 12) it clearly appears that the flow structure is not altered by the presence of the wheel and of the other obstructions around the disc. But these obstructions strongly reduce the vented mass flow rate. They also give reduced turbulence levels that are more uniformely distributed over the channles cross section, probably indicating a stronger mixing inside of the passages.

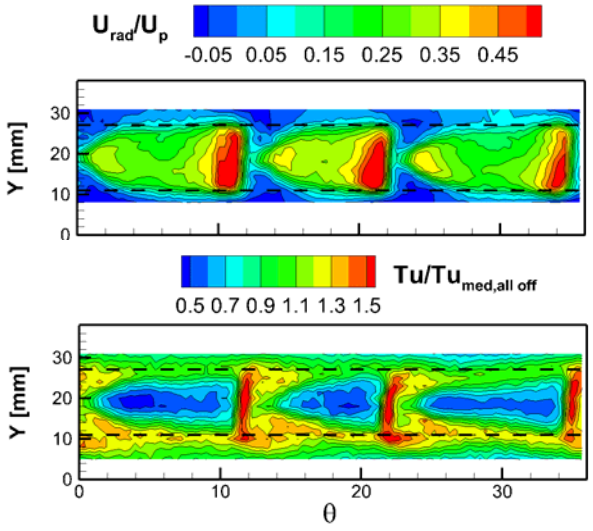

Figure 13 (a) Radial velocity and (b) Turbulence intensity distributions at 1000 rpm on the original test rig.

5.3. Experimental versus CFD results

The numerical results are now compared with the experimental data sets in terms of radial velocity distribution at distance of 4 mm from channel outlet as shown in Figure 14 (a). The redial velocity component has been normalized with respect to the peripherical speed U_p. Comparison of Fig. 14a against Fig. 10 (a) &10 (b) revealed the capability of k-ε turbulence model to predict the flow behavior inside ventilation channels. However, for example, looking at the middle channel, CFD seems to overpredict the radial velocity in the wake region while it underestimates it at the channel boundaries. Finally, the measured turbulence intensity (Fig. 11 (a) & 11 (b)) and the computed turbulent kinetic energy reported in Fig. 14 (b) have been compared although these two parameters are only comparable qualitatively due to their different definition. However, this comparison is of value for a precise CFD prediction of heat transfer coefficient. In other words, the more precise turbulent kinetic energy is predicted by CFD simulation comparing to the measured turbulence intensity, the more CFD is reliable to predict the convective heat transfer coefficient. In this study, turbulent kinetic energy distribution (Fig. 14 (b)) predicts a similar structure as the measured turbulence intensity (Fig. 11a &11b), i.e. it indicates the high turbulence regions corresponding to the wake region as well as the high turbulence regions located at the boundaries between jets and external air.

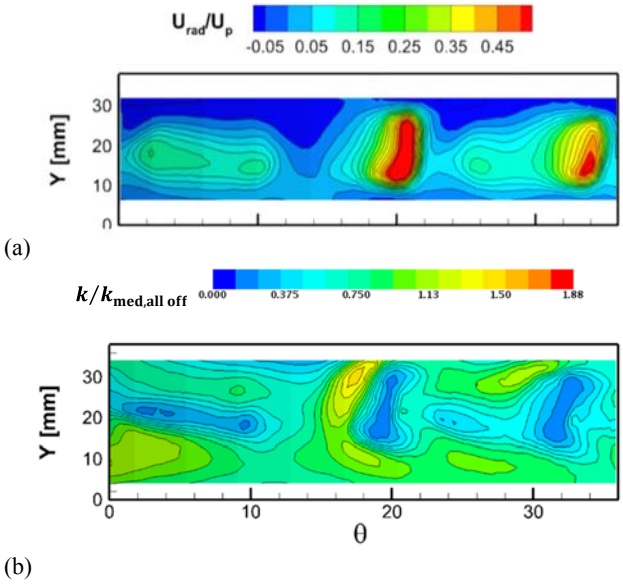

Figure 14 (a) Radial velocity and (b) Turbulence kinetic energy with forced convection- CFD prediction.

6. Conclusion

In this study, the design of an aero-dynamic bench to be representative of a car front wheel, for testing vented brake discs has been firstly investigated by means of numerical analysis in terms of heat transfer coefficient. The selected and finalized layout has been used to realize an aero-dynamic bench in the laboratory by adding different components and air lines to an existing test rig. Following that, the aero-dynamic bench has been verified through assessing each air line mass flow rate and their influence on the disc vented air by means of LDA technique. After verifying the cooling lines, a CCM standard vented brake disc has been mounted on the test bench to investigate the vented airflow field in the presence of forced convection at a fixed rotational speed of 1000 rpm. Experimental investigations confirmed previous data available in the open literature regarding vented brake discs, i.e., the vented airflow field follow a jet & wake behavior inside all three channels. The presence of forced convection leads to a slightly decrease in radial velocity as well as turbulence intensity distribution. Furthermore, the presence of the wheel and other obstruction strongly impacts on the vented mass flow rate as well as on the turbulence intensity level that hves been both reduced. Finally, predictions from k-ε turbulence model were compared against measurements of radial velocity, as well as turbulence intensity. One could conclude that a steady RANS approach could properly capture the jet behavior inside ventilation channels. Further research should include the measurement of the aerodynamic and thermal performance of vented rotors under braking conditions. This is part of an ongoing research.

Nomenclature

k	Turbulent Kinetic Energy, [J/Kg]
$\dot{m}$	Air mass flow [g/s]

T	Temperature, [°C]
Tu	Turbulence Intensity,[%]
U	Velocity, [m/s]
Y, Θ, r	cylindrical coordinate system
ε	Turbulent energy dissipation rate ,[J/kg.s]
μ	Dynamic viscosity, [Pa.s]
ρ	Density, [kg/m^3]
ω	Angular velocity, [rad/s]

subscripts

rad	Radial
tan	Tangential
p	peripheral

Abbreviations

CAD	Computer Aided Design
CCM	Carbon-ceramic Material
CFD	Computational Fluid Dynamic
CWT	Cold-wire Thermometry
HTC	Heat Transfer Coefficients
HWA	Hot-wire Anemometry
LDA	Laser Doppler Anemometry
PIV	Particle Image Velocimetry
RANS	Reynolds-averaged Navier Stokes
STD	Standard

References

[1] Barigozzi, G., Cossali, G.E., Perdichizzi, A., Boden, A., Pacchiana, P., Experimental Investigation of the Mean and Turbulent Flow Characteristic at the Exit of Automotive Vented Brake Discs, 2002, SAE Paper 2002-01-2590.

[2] Barigozzi, G., Cossali, G.E., Perdichizzi, A., Lorenzo, S., Pacchiana, P., Experimental Investigation of the Aero-thermal Characteristics at the Exit of an Automotive Vented Brake Discs, 2003, SAE Paper 2003-01-3338.

[3] Barigozzi, G., Perdichizzi, A., Pacchiana, P., Goller, R., Aero-thermal Characteristics of an Automotive CCM Vented Brake Discs, 2006, SAE Paper 2005-01-3930, SAE Transactions Journal of Passenger Cars-Mechanical Systems Journal, Section 6- V. 114, pp.3053-3062.

[4] Johnson, D., Sperandei, B., Gilbert, R., Analysis of the Flow Through a Vented Automotive Brake Rotor,2003, Journal of Fluids Engineering, Vol. 125, pp. 979-986.

[5] Parish. D., MacManus, G., Aerodynamic Investigations of Ventilated Brake Discs, 2005, Proceedings of the Institution of Mechanical Engineers, Part D: Journal of Automobile Engineering, Vol 219, No. 4, pp. 471-486.

[6] Jones, R.A., Cormier, P.L., Shih, T. ,Modeling of an automotive Brake Rotor, 1995, SAE Paper951116.

[7] Krusemann, R,, Schmidt, G., Analysis and Optimization of Disc Brake Cooling via Computational Fluid dynamics. SAE Paper 950791.

[8] Voller, G., Tirovic, M., Morris, R., and Gibbens, P., Analysis of Automotive Disc Brake Cooling Characteristics, 2003, Proc. Instn. Mech. Engrs.,Part D: Journal of Automobile Engineering, Vol 217, pp. 657-666.

[9] Barigozzi, G., Perdichizzi, A., Donati, M., Combined Experimental and CFD Investigation of Brake Discs Aero-thermal Performances, 2008, SAE paper 2008-01-2550.

[10] Watkins, S., Stephens, A., Dixon, Ch., the Aerodynamics of Vented Disc Brakes, 2005, European Automotive Congress , EAECO5YU-AS05.

[11] https://thesteveportal.plm.automation.siemens.com/

[12] https://documentation.thesteveportal.plm.automation.siemens.com/starccmplus_latest_en/index.html?param=aLKHC&authLoc=https://thesteveportal.plm.automation.siemens.com/AuthoriseRedirect#page/STARCCMP%2FGUID-B55A7D91-D613-4E1E-A7C2-133B3260A16B.html%23

[13] Stephen B. Pope, Turbolent Flows, seventh printing 2010 (first edition 2000); 369-385.